Nano Energy 148 (2026) 111701

Contents lists available at ScienceDirect

Nano Energy

journal homepage: www.elsevier.com/locate/nanoen

Walking-induced triboelectric charges by grounding release for accelerating wound self-healing

Yongfang Ren [a,1], Lin Luo [a,1], Tian Le [a], Lingling Xu [a], Engui Wang [b], Jing Huang [c], Zhipeng Qu [a], Xu Wu [a], Linqin Peng [d], Haoran Liu [a], Wenzheng Feng [a], Xiangjie Xu [a], Dongjie Jiang [e], Xia Wang [d], Bojing Shi [f], Hongqing Feng [b], Zhou Li [g], Han Ouyang [a,*]

[a] School of Nanoscience and Engineering, School of Chemical Sciences, University of Chinese Academy of Sciences, Beijing 100049, China
[b] College of Materials Science and Opto-Electronic Technology, University of Chinese Academy of Sciences, Beijing 100049, China
[c] Beijing Institute of Nanoenergy and Nanosystems, Chinese Academy of Sciences, Beijing 101400, China
[d] The Key Laboratory of Land Resources Evaluation and Monitoring in Southwest China, College of Geography and Resources, Sichuan Normal University, Chengdu 610066, China
[e] Department of Advanced Manufacturing and Robotics, College of Engineering, Peking University, Beijing 100871, China
[f] Key Laboratory for Biomechanics and Mechanobiology of Chinese Education Ministry, Beijing Advanced Innovation Centre for Biomedical Engineering, School of Biological Science and Medical Engineering, Beihang University, Beijing 100191, China
[g] Beijing Tsinghua Changgung Hospital, School of Clinical Medicine, School of Biomedical Engineering, Tsinghua Medicine, Tsinghua University, Beijing 100084, China

ARTICLE INFO

Keywords:
Triboelectrification
Grounding
Self-powered
Accelerate self-healing

ABSTRACT

Electrical stimulation systems can enhance endogenous electrical fields to accelerate and guide wound self-healing. However, the patient comfort and compliance are limited by a reliance on the stimulators and energy supply. Here, we propose a walking-induced triboelectric charges method for accelerating wound self-healing by forming a closed loop through grounding without any electronic devices or energy supply. The walking-induced triboelectric charges of human can exceed 50 V in voltage and 1 μA in current that sufficient for accelerating wound self-healing. In the proof-of-concept experiment, triboelectric charges generated during rat movement are utilized for accelerating the wound healing by enhancing the endogenous electric field (EF) of the wound. Accelerated wound self-healing was observed compared to the control group and further confirmed by tissue sectioning and transcriptomic analysis. This wound electrical stimulation repair method without electrical stimulators and power sources that potentially providing emergency care for patients in extreme situations, such as deep space or the deep sea, and offering medical convenience for people in resource-poor regions.

1. Introduction

Millions of patients suffer from chronic non-healing wounds and large-area open wounds following skin injuries every year [1]. Accelerating the healing of skin wounds is crucial for the patient's rehabilitation, as the skin serves as the primary defense against external physical, chemical and biological invasions [2,3]. Electrical stimulation is a highly promising nonpharmacological treatment method that can effectively accelerate wound healing and tissue regeneration through enhancing the endogenous electric field (EF) [4–7]. The electric field can guide the repair cells to migrate from the wound edge to the center of the wound due to the electrotactic effect, thereby accelerating re-epithelialization and tissue repair [8,9].

Traditional electrical stimulation equipment is bulky in size, thus patients can only receive short-term treatment at specific locations [10]. Then, wearable electronic devices have overcome this drawback and realized in-situ continuous electrical stimulation treatment [11–13]. Recently, self-powered devices eliminate power supply through energy harvesting to improve patient benefits and compliance [14–19]. They showed distinguished advantages in the healing of wound, such as piezoelectric nanogenerators [20], ultra-flexible and biocompatible photoelectric patch [21], magnetoelectric wound dressing [22], and thermoelectric reaction-type dressing [23]. Especially, triboelectric nanogenerators (TENGs) also bring new possibilities for electrically

* Corresponding author.
E-mail address: ouyanghan@ucas.ac.cn (H. Ouyang).
[1] These authors contributed equally

https://doi.org/10.1016/j.nanoen.2026.111701
Received 19 November 2025; Received in revised form 25 December 2025; Accepted 2 January 2026
Available online 3 January 2026

stimulated wound healing. Li et al. [24] utilized functional hydrogel-based TENG to promote wound healing and capture electrical signals during healing process. The group of Miao [25] was the first to integrate TENG into the wound dressing made of DNA hydrogel, creating a well-ordered bioelectricity. Kuo et al. [26] proposed a surface charge improved single electrode mode TENG for EF assisted wound healing applications. However, the need for functional materials, electronic devices and additional energy sources limited their broader application, especially in extreme situations and resource-poor regions [8,27].

Generally, the human daily activities generate huge amount of triboelectric static charges, which always leading negative impacts in human health, industrial manufacturing and transportation [28–30]. However, as a potential energy source, the benefits of triboelectric charges are usually overlooked. Fortunately, Shi et al. [31] presented a body-integrated self-powered system, which can scavenge energy from human motions to power bioelectronic devices. Kang et al. [32] provided a technology that may prevent the spread of virus based on walking-induced electrostatic charges harvesting. Kim et al. [33] also reported that contact electrification enables in situ electroporated disinfection in portable water bottles. These works demonstrated that the human body can serve as both a power source and a part of the circuit, almost eliminating all limitations on energy supply to achieve self-powering [34–37]. Furthermore, it has been reported by Khayamian et al. [38] that triboelectric charges were delivered through conductive pathways to promote wound healing. As the rat continued to walk, the charge generation alternated between the left and right sides, leading to a natural EF stimulation across the wound site.

Inspired by endogenous electric fields promoting wound self-healing, we propose a walking-induced triboelectric charges method for accelerating wound self-healing by forming a closed circuit through grounding without any electronic devices or energy supply. The walking-induced triboelectric charges of human can exceed 50 V in voltage and 1 μA in current. In the proof-of-concept experiment, triboelectric charges generated during rat movement are utilized for accelerating the wound healing by enhancing the endogenous electric field of the wound. The point-of-use method operates without an external power supply, should provide an energy-autonomous and drug-free repair strategy for the healing of wounds.

2. Results

2.1. In vitro output test

The structure of the device mainly consists of commercial hydrogel patch, the silicone tube filled with hydrogel, and metal wire. The silicone tube filled with ionically conductive hydrogel can efficient delivery of the triboelectric charges (Fig. S1a), the embedding metal wire was used as the contact electrode and provided stable grounding pathway (Fig. S1b), and the hydrogel patch can be easily attached to the human skin (Fig. S1c).

The working principle of the in vitro test leverages triboelectric charges generated on shoes through contact and separation between the shoes and the floor during human motion. Due to the difference in triboelectric polarities between the shoes and the floor, static electricity can be generated on the human body during movement through friction. During the process of movement, electrons transfer from the surface of floor to the sole of the shoes, causing the sole to accumulate static electrons, while the floor surface left an equal number of positive charges. When the sole of a shoe was lifted, the body electric potential was established between the human body and the floor. If a load (the hydrogel–silicone tube–metal wire device) was connected to the human body and the ground, the free electrons will flow from the human body to the ground to balance the potential difference, thereby causing the foot to carry positive charges. When the sole moving close to the floor led to an opposite body electric potential change, causing a reversed electron flow from the ground to the human body. Furthermore, the current signals generated when lifting the foot and putting the foot down were not identical, because the velocity when the foot was put down was slightly higher than that when the foot was lifted (Fig. 1a). The contact separation between the human body and the ground alternately causes the accumulation and release of static charges, thereby generating electrical energy [39]. These charges accumulate on the body surface and were driven via the hydrogel–silicone tube–metal wire pathway, forming a closed loop with the ground (Fig. 1a).

To evaluate the output performance, conductive hydrogel patches were attached to the skin of participants and connected to an electrometer. The clothing material was used as the insulating layer, and the materials that constitute the clothing, as long as they have insulating properties, had almost no impact on the output performance [30]. We investigated the effect of contact area on in vitro electrical output using ethylene vinyl acetate copolymer (EVA), a primary material for manufacturing shoe soles. The results indicated that short-circuit current (I_{SC}) increased with larger contact area, while open-circuit voltage (V_{OC}) remained largely unaffected (Table S1). The relationship between the output and electrodes located at various body parts and the distance (wire-ground) was also investigated. We found that the output when different body parts including the hand, arm, crus, thigh, and shoulder came into contact with the hydrogel was not significantly different. Moreover, when the resistance of the wire was sufficiently low, the distance between the wire and the ground did not affect the electrical output (Table S1). The I_{SC} and V_{OC} measured under three different activities (walking, running, and stepping) were shown in Fig. 1b. It can be seen that I_{SC} reached approximately 0.5 μA during walking and increased to about 2 μA during running and stepping. As the frequency of the movement increased, the short-circuit current value exhibited an increasing trend, which was attributed to the increased charge flow rate resulting from the higher frequency [40]. Additionally, V_{OC} showed an increase from ~80 V during walking to ~110 V during running. Compared to the I_{SC}, the V_{OC} change was not significant, all remaining around 100 V. Experimental results confirmed that increasing the intensity of motion enhanced the accumulation of triboelectric charges and the electrical output. Furthermore, during the stepping process, output characteristics were obtained by connecting the system to different external loads (Fig. S2a). The peak power was approximately 0.44 mW with a typical internal resistance of approximately 30 MΩ, and the corresponding current under various load conditions was further calculated (Fig. S2b). These results indicate that the energy generated by triboelectrification has the potential to power small electronic devices.

To validate the universal capability to drive electronic devices, a "UCAS" pattern light board composed of 44 light-emitting diodes (LEDs) as the load. When the participant was stepping, the LED bulbs flashed rhythmically (Fig. 1c), with the corresponding current and voltage measured at ~3 μA and ~150 V, respectively (Fig. 1d). This not only validated that human-generated static electricity can drive low-power devices but also suggested potential applications in powering bioelectronic systems and regulating biological activity [41].

To gain further insight into the underlying mechanism, the potential distribution and electric field vectors throughout the entire body were further simulated by COMSOL Multiphysics simulation (Fig. 1e and Fig. S3). The simulation results verified that a high potential appeared at the feet, while grounding caused the potential at the wound site to be relatively lower (Fig. 1e). The electric field vector diagram further indicated that the direction of the electric field pointed from charge source at the foot to the grounded wound site, and the direction of the current was consistent with it (Fig. S3). This potential difference arises from repeated frictional contact and separation, highlighting the spatial characteristics of charge accumulation and release when the human body acts as a conductor.

Given that individual variation may affect energy harvesting, external outputs were also tested in different participants during stepping, and peak current, voltage, and charge values were recorded

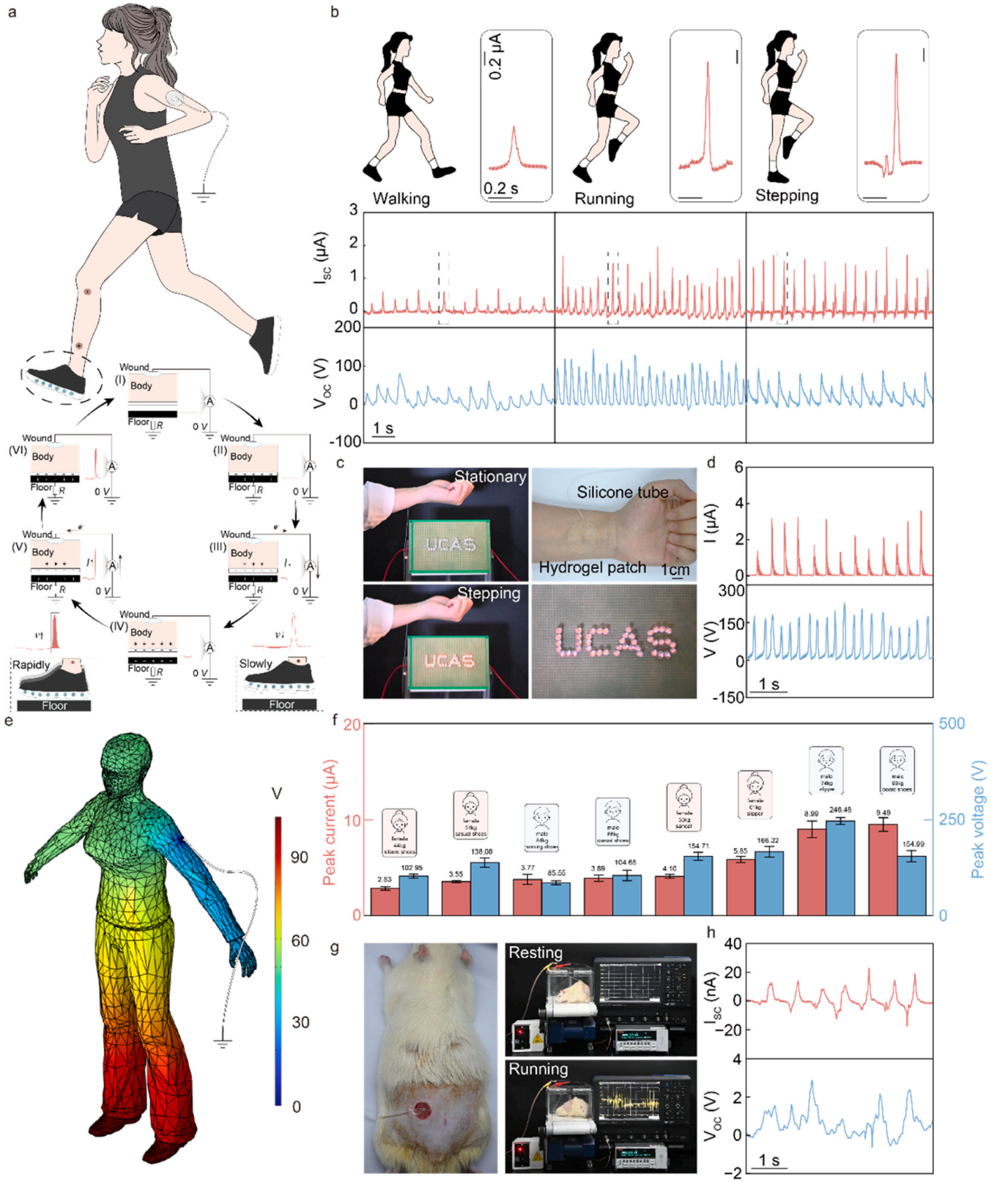

Fig. 1. Typical output characteristics of the walking-induced triboelectric charges. (a) Schematic illustration of energy output based on human movement and the working principle based on the triboelectric mechanism. (b) The short-circuit current (I_{SC}) and open-circuit voltage (V_{OC}) output when a participant was walking, running or stepping. (c) The energy from the steps was enough to light up the LEDs. (d) The current and voltage output recorded while stepping to light up LEDs. (e) Simulation the potential distribution throughout the entire body by COMSOL Multiphysics simulation. (f) Statistics of peak current (red) and peak voltage (blue) from different participants during stepping. (g) Signal output during the resting and running processes of rats. (h) The short-circuit current and open-circuit voltage measured when a rat was running.

(Fig. 1f and Fig. S4). Inter-individual differences in output were observed during walking, which could be attributed to variations in foot–ground contact properties, contact area, and typical internal resistance [31]. Despite these differences, peak currents for all participants remained in the range of a few microamperes, and peak voltages were around one to two hundred volts, indicating that the system reliably generates sufficient electrical output to power small electronic devices across different individuals.

Finally, the system was applied to a rat with a dorsal wound to further assess its potential for wound applications (Fig. 1g). Signals recorded from the rat under resting and running states showed I_{SC} and V_{OC} values of ~20 nA and 2.5 V, respectively (Fig. 1h). Although the energy output was lower than in humans, the stable signals demonstrated that walking-induced triboelectric charges could be effectively harvested in small animal models, highlighting the feasibility of using grounding intervention to stimulate wound healing.

2.2. Cell migration and biological safety assessment

To evaluate the potential of triboelectric charges for promoting

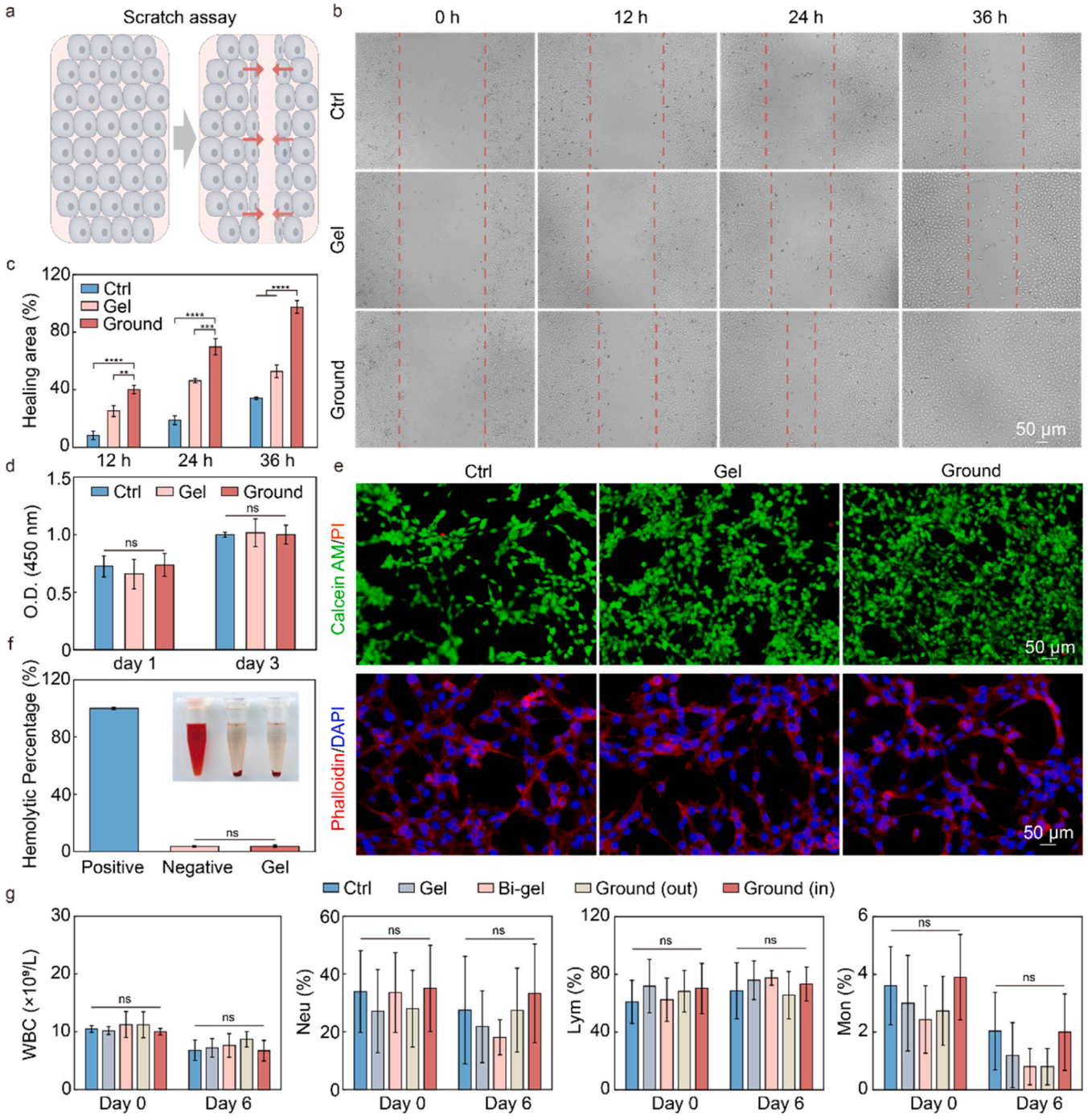

Fig. 2. Cell migration and biological safety assessment. (a) Schematic diagram of scratch assay. (b) Representative 3T3 cell migration images at different time points. (c) Statistical graph of cell healing area (n = 3). (d) CCK-8 cell viability assay at day 1 and day 3 (n = 3). (e) Live/dead cell staining using Calcein AM (green) and PI (red) at day 3 and cell skeleton staining with Phalloidin (red) and nuclear staining with DAPI (blue) at 48 h. (f) Hemocompatibility assessment comparing positive control, negative control, and hydrogel (n = 3). (g) Blood routine related indicators of rats at day 0 and day 6 (n = 3).

wound healing and assess the biological safety of the hydrogel under electrostatic stimulation, we performed a series of in vitro cell migration and biocompatibility assessments. These experiments were designed to examine the influence of an electric field simulating rat movement on cellular behavior, as well as to verify the safety of the material for potential wound healing applications [42,43].

Cell migration was evaluated using the scratch assay to mimic the wound healing process (Fig. 2a). A signal generator was used to simulate the electrical signal (V_{OC}) induced by the walking of rats to provide electrical stimulation for cell migration. As shown in Fig. 2b, after 36 h, the ground group exhibited complete wound closure. The quantitative results (Fig. 2c) indicated that after 24 h of electrical stimulation, the percentage of healed area in the ctrl group, gel group and ground group was approximately 18.94 %, 46.36 % and 69.89 % respectively. The healed area of the ground group was about 3.69 times that of the ctrl group, confirming that electrostatic stimulation significantly enhanced cell migration.

Further analysis was performed using the CCK-8 cell viability assay, live/dead staining, and cytoskeleton staining to evaluate cell compatibility of hydrogel with and without electrical stimulation [44]. The CCK-8 results showed no significant differences in optical density (O.D.) at 450 nm between the groups at day 1. Over 3 days, O.D. values increased in all groups, indicating normal cell proliferation and confirming that the hydrogel, with or without electrical stimulation, exhibited no cytotoxic effects (Fig. 2d). The live/dead cell staining experiment further confirmed the result. As shown in Fig. 2e and Fig. S5, the cells in the ground group maintained a high survival rate, and the number of live cells was much greater than that of dead cells. The analysis of cell cytoskeleton staining showed well-spread morphology and strong adhesion after electrical stimulation, confirming excellent cytocompatibility without adverse effects from the applied field (Fig. 2e and Fig. S6).

Furthermore, we investigated the blood compatibility of hydrogel (Fig. 2f). The hemolysis rate was 3.67 %, comparable to the negative control and well below the 5 % threshold, confirming the safety of the material in blood contact without inducing hemolysis [45]. During the treatment process, we conducted blood routine and blood biochemical tests on each group of animals (Fig. 2g, Fig. S7 and S8). The blood test results showed that there was no significant difference between the material, grounding and control group, further supporting the in vivo safety of both the hydrogel and the electrostatic stimulation.

2.3. Grounding intervention accelerated full-thickness wound repair in rat

To systematically evaluate the impact of body's triboelectric charges and current direction on wound healing, a 1 cm circular full-thickness skin defect was created on SD rats and divided into five groups: Ctrl, Gel, Bi-gel, Ground (in), and Ground (out) group. The wound center or edge was coated with hydrogel, which was used for grounding at the wound center or edge. COMSOL Multiphysics simulation was performed to better understand the influence of the grounding position on the distribution of the electric field at the wound site. The electric potential and electric field intensity at center or edge of the wound by grounding were shown in Fig. S9. It can be seen that grounding caused the center of the wound to have a lower electric potential, which was more conducive to guiding the repair cells to migrate from the wound edge to the center of the wound, thereby accelerating tissue repair. Throughout the healing process, grounding intervention was applied for 9 days (Fig. 3a). The schematic diagram and wound healing mechanism of the rat grounding model were shown in Fig. 3b. Similar to the human demonstration, the conductive hydrogel patch was applied to the wound site of the rat, and the triboelectric charges were generated by the friction between the rough paws of the rats and the rubber. During the movement of the rat, the rat carried positive charges, and accordingly, the rubber acquired electrons and became negatively charged. The grounding of the wound caused positive charges to flow out, accelerating the healing of the wound. The wound images were taken every 3 days to dynamically monitor closure (Fig. 3c). Tissue samples were collected on day 6, 12, and day 21 post-injury for transcriptomic and histological analysis, providing in-depth insights of grounding intervention in promoting tissue repair. Among all groups, the Ground (in) group demonstrated the most significant healing effect. On day 3, the wound healing rate of Ground (in) group was larger (40.22 %) compared with control (15.22 %), Gel (25.31 %), Bi-gel (28.03 %), and Ground (out) (31.94 %) (Fig. 3d). This was attributed to center grounding, which allowed the triboelectric charges to flow out from the center of the wound. The potential difference between the center and the edge of the wound increased, thereby enhancing the EF of the wound. In addition, the body weight of all experimental rats remained stable and H&E staining of vital organs showed no signs of pathological changes, confirming the safety and effectiveness of the grounding intervention in promoting wound healing (Fig. S10 and S11).

To further investigate the histological changes associated with grounding intervention during wound healing, we performed H&E and Masson staining at different time points. On day 6, H&E staining images revealed that the length of the newly formed epidermis in the Ground (in) group reached 5.12 mm, which was significantly longer than the 1.5 mm observed in the other groups (Figs. 3e and 3f). By day 12, the Ground (in) group exhibited the narrowest granulation tissue (Fig. S12a), with a width of only 1.08 mm (Fig. S12b), significantly smaller than in the other groups. This suggests that grounding intervention not only accelerated the initial stages of tissue repair but also promoted the faster maturation of granulation tissue, which is crucial for wound closure. Furthermore, Masson staining on the 12th day (Fig. S12c) revealed the presence of abundant rete pegs in the Ground (in) group, which played an important role in the differentiation, growth, and repair of epithelial cells [46].

On day 21, the skin structure in the Ground (in) group was restored relatively completely, with an epidermal thickness of 63.98 μm, almost double that of the control group (31.74 μm) (Figs. 3e and 3g). This indicated that grounding intervention had a significant promoting effect on skin regeneration. Masson staining on day 12 (Fig. S13a) revealed that collagen fibers in the Ground (in) group were more densely packed and more uniformly organized, while fibers in the other groups were arranged more loosely. Quantitative results (Fig. S13b) further indicated that the collagen volume fraction in the Ground (in) group was higher (78.17 %), compared to the Control (64.22 %), Gel (65.69 %), Bi-gel (69.98 %), and Ground (out) (67.79 %) groups, indicating enhanced extracellular matrix deposition and tissue maturation.

Macrophage polarization in the wound was further evaluated using CD86 and CD206 immunofluorescence to examine the effect of grounding-induced electrical stimulation on the inflammatory microenvironment. CD86 and CD206 are the markers M1 and M2 type macrophages respectively [47]. On day 6, the Ground (in) group exhibited stronger CD206 (M2) signals (Fig. 3h), and quantitative analysis showed a significantly higher M2/M1 ratio (2.48) compared to the Ctrl (0.13), Gel (0.24), Bi-gel (0.40), and Ground (out) (0.41) groups (Fig. 3i), suggesting that electrical stimulation promoted the transformation of macrophages from the pro-inflammatory M1 phenotype to the anti-inflammatory and pro-healing M2 phenotype during the healing process [48].

To assess the impact of grounding-induced electrical stimulation on tissue repair, angiogenesis was evaluated using CD31 immunofluorescence staining, a marker for endothelial cells. Immunofluorescence staining showed that the $CD31^{+}$ vascular area per high power field (HPF) of the Ground (in) group increased approximately 6-fold and 2-fold compared to the Ctrl/Gel group and Bi-gel/Ground (out) group, respectively (Figs. 3h and 3j). This indicated that grounding at the center can effectively promote the formation of new blood vessels, providing better nutrition and oxygen supply for tissue repair [49]. The M2 type macrophages are important angiogenic cells, consistent with the finding that an increase in M2 macrophage numbers promoted the formation of

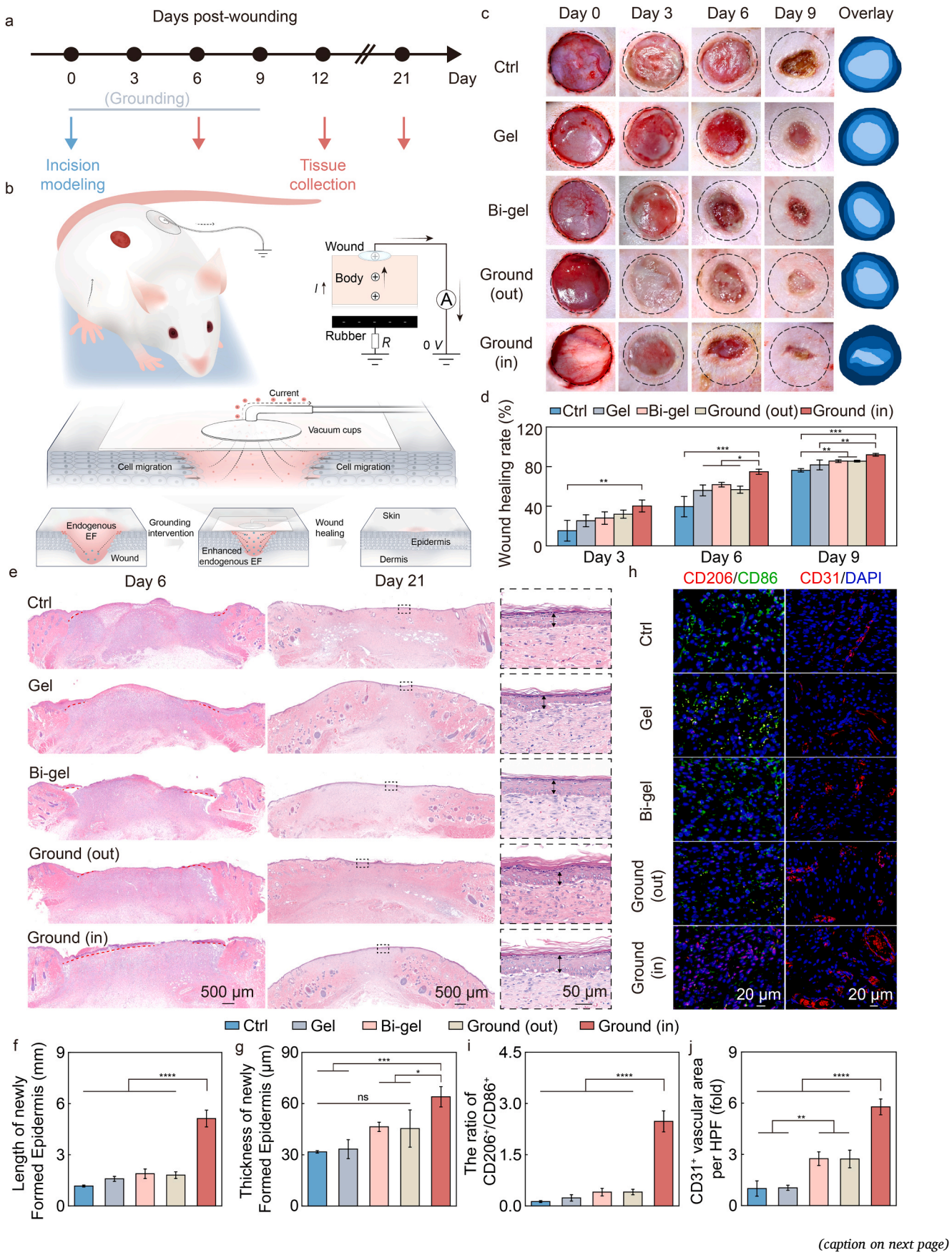

(caption on next page)

Fig. 3. Grounding intervention accelerated full-thickness wound repair in rat. (a) Schematic diagram of the rat model of wound healing by grounding intervention. (b) Schematic diagram and wound healing mechanism of the rat grounding model. (c) Representative images showing wound repair at different time points (the diameter of the original wound was 1 cm). (d) Statistical data of the percentage of wound healing over time (n = 3). (e) H&E staining of wounds in different experimental groups on the 6th day and the 21st day. (f) Statistical analysis of length of newly formed epidermis in different experimental groups on the 6th day (n = 3). (g) Statistical analysis of thickness of newly formed epidermis in different experimental groups on the 21st day (n = 3). (h) Immunofluorescence staining of each experimental group on the 6th day and the 12th day, showing CD206 (red) and CD86 (green) for macrophages, and CD31 (red) for endothelial cells. (i) Statistical analysis of the ratio of $CD206^+$ /$CD86^+$ in different experimental groups on the 6th day (n = 3). (j) Statistical analysis of the $CD31^+$ vascular area per high power field (HPF) in different experimental groups on the 12th day (n = 3).

blood vessels. These results demonstrated that electrical stimulation can effectively regulate the inflammatory microenvironment, promote angiogenesis, and thereby accelerating wound healing.

2.4. Transcriptome analysis

To further elucidate the molecular mechanisms underlying the enhanced wound repair observed in histological analyses, transcriptomic profiling was performed on wound tissues from the control (Ctrl, C), material (Bi-gel, M), and grounding (Ground (in), G) groups. On the sixth day, the length of the newly formed epidermis in the Ground (in) group surpassed that of other groups and macrophages transformed from the M1 phenotype to the M2 phenotype. This stage marks the critical transition of the wound from the inflammatory phase to the proliferative phase. Heatmaps revealed distinct expression patterns between Ground (in) and the Ctrl or Bi-gel groups, highlighting a set of differentially expressed genes (DEGs) (Figs. 4a and 4b). The Upset plot further illustrated the overlap and distribution of these DEGs among different groups (Fig. 4c). Kyoto Encyclopedia of Genes and Genomes (KEGG) enrichment analysis (Figs. 4d and 4e) indicated that grounding intervention pathways associated with stem cell proliferation (Cytokine-cytokine receptor interaction), promoted the regulation of intracellular calcium homeostasis (Calcium signaling pathway), and affected inflammatory response and tissue repair (IL-17 signaling pathway). The Heatmap of key genes (Fig. 4f) showed that there are more differential genes related to wound repair in the Ground (in) group compared with the Ctrl and Bi-gel groups. The genes upregulated in the Ground (in) group were labeled in the Volcano plot (Fig. 4g). The inflammation protection mediated by Cryab/Hspb7 paves the way for repair. Subsequently, enhanced cell adhesion via Actn2, neural regulation via Pvalb/Cryab, and angiogenesis initiated by Ccl21/Ampd1/Hspb7 ensure nutrient supply. Ultimately, the extracellular matrix (ECM) constructed by Col7a1/Col19a1 enables the stable restoration of structure and function, which consistent with the increased collagen deposition observed by Masson staining (Fig. S13). The upregulation of these genes constitutes the molecular basis for grounding intervention to accelerate wound self-healing.

Gene set variation analysis (GSEA, Fig. 4h-k) further verified the activation of the enriched signaling pathways. Among them, the Calcium signaling pathway, ECM-receptor interaction and Hedgehog signaling pathway were all upregulated in Ground (in) group, while the Interleukin 17 (IL-17) signaling pathway was downregulated. The activation of the Calcium signaling pathway and ECM–receptor interaction suggests enhanced regulation of intracellular calcium homeostasis, cell adhesion, and extracellular matrix remodeling—processes critical for cell migration, proliferation, and tissue re-epithelialization. The Hedgehog pathway upregulation indicated promotion of stem cell activity and tissue regeneration. IL-17 is a highly versatile pro-inflammatory cytokine that is essential for host immune defense [50], its suppression indicated the success of inflammation inhibition during the early healing stage. Consistent with a significant increase in the M2/M1 ratio during the healing process, this indicated that electrical stimulation created a favorable immune microenvironment for wound healing. Overall, these results suggest that grounding intervention may facilitate wound healing via multiple regulatory pathways by enhancing tissue regeneration, stabilizing the extracellular environment, and regulating the inflammatory microenvironment.

3. Discussion

In conclusion, we proposed a method for harnessing the walking-induced triboelectric charges of the human body, which achieved charge flow through grounding, and accelerated the wound self-healing. We systematically evaluated the promoting effect of the triboelectric charges of the human body on wound healing in vivo and verified the influence of the current direction on the endogenous EF within the wound. Grounding at the center of the wound can effectively enhance the endogenous EF, which in turn modulated gene expression and signaling pathways associated with tissue regeneration, extracellular matrix stability, and inflammatory response, thereby promoting efficient and orderly wound repair. The point-of-use method operated without external power supply, relying entirely on the triboelectrification, which makes it suitable for emergency applications in extreme environments (deep space, deep sea, even the moon and mars) as well as offering medical convenience for people in resource-poor regions. In addition, the concept of grounding intervention could be combined with any materials approved by the Food and Drug Administration (FDA) and even be expected to be integrated with negative pressure wound treatment (NPWT). This will contribute to novel strategies for healing chronic wounds with excessive exudate in clinical practice, expand the application group, and promote the development of the medical industry. All in all, the triboelectric charges of the human body were utilized to accelerate wound self-healing, providing an energy-autonomous and drug-free repair strategy for the healing of wounds.

4. Materials and methods

4.1. Material

The hydrogel patches/hydrogels and Tegaderm transparent dressings were purchased from Coloplast and 3 M company, respectively.

4.2. Electric measurements

The output current and voltage of human/rat movement were measured using an electrometer (Keithley 6517B) and an oscilloscope (LeCroy, HDO6104). In the human demonstration experiment, the triboelectric charges originated from the friction between the sole of the shoes (ethylene vinyl acetate copolymer, EVA) and the floor (tile). In the demonstration experiment on rats, the triboelectric charges were generated by the friction between the rough paws of the rats and the rubber.

4.3. COMSOL Multiphysics simulation

The COMSOL Multiphysics simulation was based on version 6.3 and was used to simulate the electric field distribution in the wound to assess the impact of potential and electric field intensity on wound healing. The simulation process began with model construction, where the three-dimensional geometry of the human model was created using 3D Max software. This model included the main anatomical features of the human body to ensure the biological authenticity of the geometric shape. Then, the human model was imported into the COMSOL environment and a wound model was further drawn based on it. Specifically,

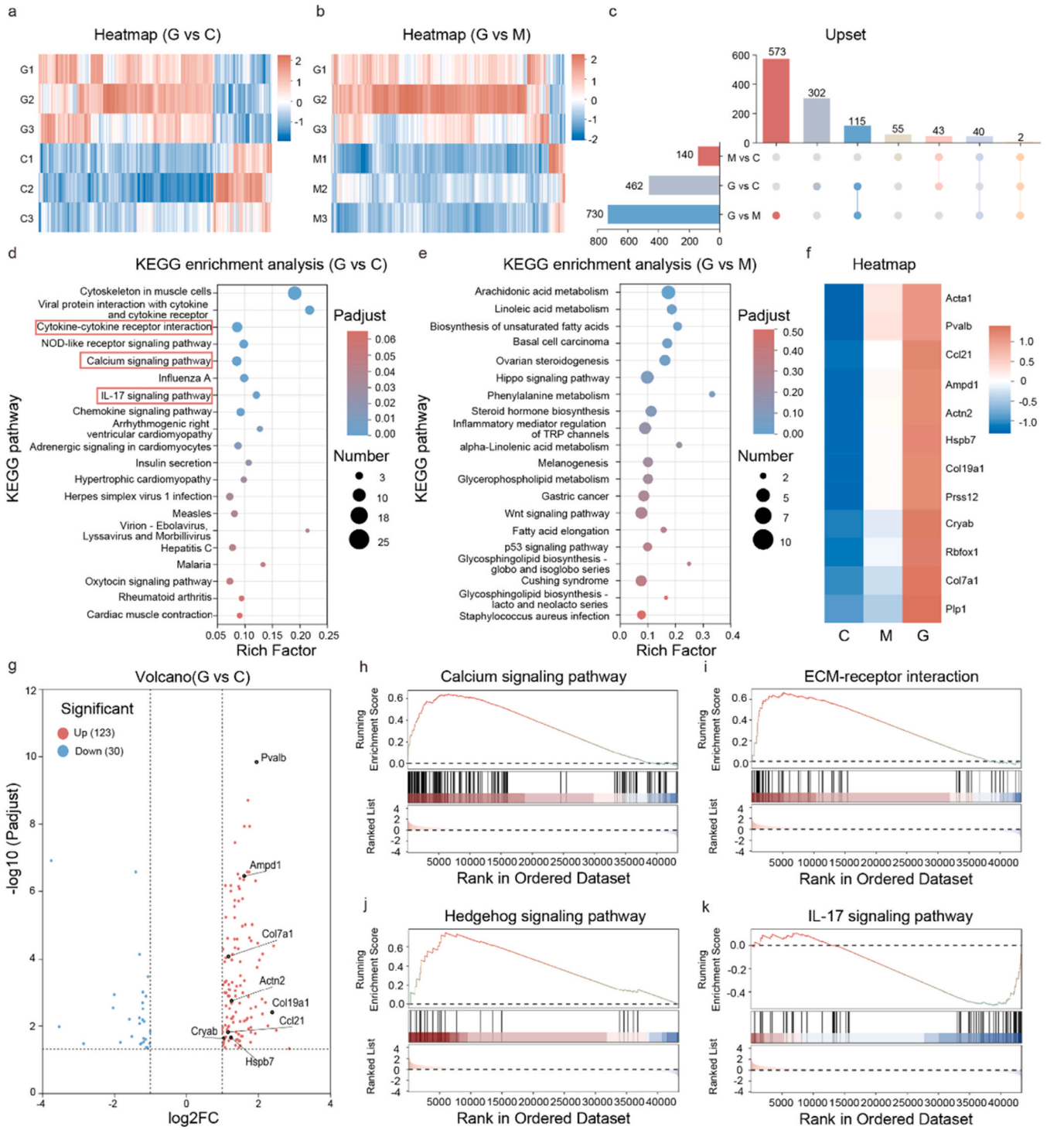

Fig. 4. Transcriptome analysis of wound tissue at 6 days. (a) Differential gene enrichment heatmaps for the ground (in) group (G) relative to the ctrl group (C), and (b) relative to the materials group (M). (c) Upset plots of shared and unique genes between groups. (d, e) Bubble plots of KEGG enrichment analysis of DEGs in the Ground (in) group compared with the Control group (d) and Bi-gel group (e). (f) Heatmap of genes related to healing in different groups. (g) Volcano maps of differential gene enrichment in the ground (in) group relative to the ctrl group. (h–k) Gene set variation analysis (GSEA) of the Calcium signaling pathway (h), Extracellular matrix (ECM)–receptor interaction (i), Hedgehog signaling pathway (j), and Interleukin 17 (IL-17) signaling pathway (k).

the wound geometry was directly constructed using the built-in tools of COMSOL, with the wound modeled as a cylinder with a diameter of 1 cm, located in the area of the human model. Material properties were defined in the "Materials" node of COMSOL, specifying the electrical properties of dry skin for human tissues, including the relative dielectric constant ($\varepsilon r = 44.817$) and electrical conductivity ($\sigma = 0.599$ S/m), to reflect the electrical behavior under dry physiological conditions. The physical field settings were carried out under the "Physics" node, using the "Electrostatics" interface, enabling steady-state solving to calculate the static electric field distribution. The boundary conditions were set by determining the surface charge quantity on the human body surface (measured value: 104.49 nC), and the responses under different electric field conditions were simulated. The meshing was done using the "Physics-Controlled Mesh" method, generating a free tetrahedral mesh

under the "Mesh" node, and refining the mesh in the wound area to improve accuracy. The solution process used the "Stationary" study step, configuring the "Fully Coupled" solver, with a relative tolerance of $1e^{-4}$. After running the solution, monitoring the convergence of the potential was carried out to ensure numerical stability.

4.4. Cell culture

3T3 cells were cultured in high-glucose DMEM medium (Solarbio) supplemented with 10 % fetal bovine serum (FBS, Gibco) and 1 % penicillin-streptomycin (Solarbio). Cells were maintained in a humidified incubator at 37 °C with 5 % CO_2.

4.5. Cell migration

The wound healing process in vitro was simulated through cell scratch experiments. We employed hydrogel and electric field stimulation to investigate whether they could promote cell migration. 3T3 cells were cultured in 6-well plates until they grew fully, and a linear scratch was made using the tip of a pipette to create a cell-free gap. The cells were washed three times with phosphate buffered saline (PBS) to remove the detached cells, and the initial image of the scratch was captured under a microscope (ICX41). Subsequently, the hydrogel was added into culture medium with/without an electric field stimulation to allow cell migration, and placed them in the incubator. Graphite electrodes were inserted to both sides of the scratch, with an electrode spacing being 3 cm. A signal generator was used to simulate the electrical signal induced by the walking of rats to provide electrical stimulation until complete cell closure was achieved. Images were taken at the same position again at 0 h, 12 h, 24 h, and 36 h to record the movement of the cells towards the defect area. Finally, the images at different time points were compared and analyzed, and the cell migration was quantitatively analyzed using ImageJ software.

4.6. Cell biocompatibility

The cell viability was assessed using the CCK-8 assay (Cell Viability/Cytotoxicity Detection Kit, Solarbio). After culturing the cells for 1 and 3 days, removing the culture medium and washing with PBS, they were incubated together with the culture medium containing 10 % CCK-8 reagent in the incubator for 40 min. Then, the absorbance at 450 nm was measured using a microplate reader (Thermo Fisher Scientific). Furthermore, the biocompatibility was evaluated by the Calcein-AM/PI live/dead assay (Solarbio). 10 mg hydrogel was dissolved in 10 mL DMEM solution and stood for 24 h, resulting in leachate containing the hydrogel. After the cells were cultured in the leachate for 3 days with or without electrical stimulation, washed with PBS and incubated with the live/dead dye at 37 °C for 40 min (in the dark). The cells were washed twice with PBS to remove excess dye. Subsequently, they were observed using a fluorescence microscope (ICX41).

4.7. Cell morphology and cytoskeleton detection

We further investigated the effects of the leachate containing hydrogel and electrical stimulation on the growth state of cells. All samples that were cultured in the leachate with or without electrical stimulation for 48 h were fixed in 4 % paraformaldehyde (Solarbio) at room temperature for 10 min. After washing with PBS, samples were subjected to permeabilization treatment in 0.1 % Triton X-100 (Solarbio), with the temperature maintained at 4 °C for 5 min. After being washed with PBS, the samples were incubated with the Rhodamine-Phalloidin (Aberman; dilution ratio 1:1000) at 37 °C for 1 h. After further washing with PBS, the samples were stained with 4′,6-diamidino-2-phenylindole (DAPI; Solarbio) for 10 min, then washed three times with PBS. Subsequently, the cytoskeleton and nucleus of the stained cells were observed using ICX41 fluorescence microscope.

4.8. Hemolysis assay

The blood biocompatibility of the hydrogel was evaluated using the hemolysis assay. 1 mL fresh rat blood (male, 8 weeks old, 250 g) was placed in an anticoagulant tube, and 2 mL PBS was added for washing. The solution was centrifuged at 1000 rpm for 5 min. This process was repeated 5 times, and then the supernatant was removed, leaving the red blood cell sediment. The washed red blood cells were resuspended in 10 mL PBS as the blood working solution. Experimental group (n = 3): 200 μL blood working solution was mixed with 800 μL hydrogel leachate (1 mg hydrogel dissolved in 1 mL PBS for 3 days). Positive group (n = 3): 200 μL blood working solution and 800 μL water. Negative group (n = 3): equal amounts of blood working solution and 800 μL PBS. After incubation at 37 °C for 4 h, all samples were centrifuged at 1000 rpm for 5 min, and the images were taken and recorded. At the same time, 100 μL supernatant sample was taken from each group, and the absorbance was detected at 545 nm.

4.9. Animal models

The experiment utilized male 8-week-old Sprague-Dawley (SD) rats provided by SPF (Beijing) biotechnology Co. Ltd. All operations were conducted in accordance with the "Administrative Measures for the Ethical Review of Experimental Animals", and were approved by the Animal Ethics Committee of the University of Chinese Academy of Sciences (202403042).

The SD rats were used to establish a full-thickness skin wound model. After inhalation anesthesia with isoflurane (1–3 % concentration), the hair on the back was shaved. Under sterile conditions, a circular full-thickness wound was made using a 1 cm circular mold. The rats were randomly divided into 5 groups, with 6 rats in each group: the control group (Ctrl, without any intervention), the hydrogel patch group (Gel, commercial hydrogel patch with wound healing function), the hydrogel + hydrogel patch group (Bi-gel, hydrogels maintain wound moisture and provide a low-impedance conductive microenvironment), the Bi-gel center-grounding group (Ground (in), wound center is conductive), and the Bi-gel outer-grounding group (Ground (out), wound edge is conductive). The patches were replaced daily and wound photos were taken every three days to monitor and measure the wound healing status. For the grounding groups, the rats received grounding intervention for 1 h each day for 9 days. During the entire treatment period, each rat was fixed with Tegaderm after treatment to prevent skin contraction. Then, elastic adhesive bandages were used for fixation to prevent infection and self-inflicted harm. Finally, the wound healing rate was calculated using ImageJ software based on the wound photos taken at each time point.

4.10. Blood analysis

Blood routine and blood biochemical tests were conducted on each group of animals during the treatment process for blood analysis. During the experiment, blood samples were taken on the 0 t, the 6th and the 21st day and placed in anticoagulation tubes for blood routine tests to obtain the relevant indicators. Blood samples for the sixth day were collected using vacuum blood collection tubes. The blood was centrifuged at 2500 rpm for 15 min to separate the serum, and the supernatant was collected for testing of serum biochemical indicators.

4.11. Histological analysis

The wound tissue obtained from sampling for 6, 12 and 21 days was soaked in 4 % paraformaldehyde for fixation, then dehydrated with gradient ethanol and embedded in paraffin blocks. The thickness of section was 4 μm and further analyzed by H&E, Masson and immunofluorescence staining.

4.12. Transcriptome sequencing

Wound tissue was obtained on the sixth day of wound healing. RNA was further extracted from it using TRIzol® reagent and the sequencing was performed in Majorbio Co., Ltd. company using an Illumina Nova-Seq 6000 platform (Illumina, USA). Differential expression analysis was performed using DESeq2, and differential expression genes with $|\log2FC| \geq 1$ and FDR ≤ 0.05 (DESeq2) were considered significantly differentially expressed genes. Further analysis was conducted through the online Majorbio Cloud Platform (www.majorbio.com).

5. Statistical analysis

All data were presented as mean ± standard deviation. Quantitative image analysis was performed using ImageJ software. The analysis and plotting of other data were carried out using the Origin 2025 version and GraphPad Prism 10.0 version software. Statistical significance between experimental group and other groups was assessed by one-way ANOVA, with $p < 0.05$ considered statistically significant (*, **, ***, **** corresponding to $p < 0.05$, 0.01, 0.001, 0.0001, respectively).

Author contributions

H.O. conceived and coordinated the experiments. Y.R., L.L., L.X., E.W., D.J., X.W., B.S., H.F., and Z.L. assisted in concept development. Y.R., L.L., L.X., and E.W. conducted the materials preparation and characterization. Y.R., L.L., T.L., Z.Q., H.L., and L.P. conducted the output testing. X.W. and X.X. conducted the COMSOL Multiphysics simulation. Y.R., and L.X. conducted the cell experiment. Y.R., L.L., L.X., E.W., and W.F. conducted the in vivo animal experiments. Y.R., L.L., T.L., L.X., J.H. and X.W. processed the data and drew the figures. Y.R., L.X., and H.O. wrote the paper. All authors read and revised the manuscript.

Funding

This project was supported by National Natural Science Foundation of China grant nos. 52373256 (to H.O.), and 62004010 (to H.O.); Youth Innovation Promotion Association CAS grant no. 2023176 (to H.O.); Beijing Natural Science Foundation grant no. 7232347 (to H.O.); the Beijing Nova Program grant 2024047 (to H.O.).

CRediT authorship contribution statement

Dongjie Jiang: Writing – review & editing, Validation, Supervision. **Lin Luo:** Visualization, Validation, Software, Investigation, Data curation, Conceptualization. **Tian Le:** Visualization, Software, Investigation, Data curation, Conceptualization. **Wenzheng Feng:** Visualization, Data curation. **Xiangjie Xu:** Visualization, Software. **Yongfang Ren:** Writing – original draft, Visualization, Validation, Software, Investigation, Formal analysis, Data curation, Conceptualization. **Hongqing Feng:** Writing – review & editing, Validation, Supervision, Resources. **Engui Wang:** Visualization, Supervision, Formal analysis, Data curation, Conceptualization. **Zhou Li:** Writing – review & editing, Validation, Supervision, Resources. **Jing Huang:** Visualization, Software, Data curation, Conceptualization. **Xia Wang:** Writing – review & editing, Validation, Supervision. **Bojing Shi:** Writing – review & editing, Validation, Supervision. **Lingling Xu:** Writing – review & editing, Visualization, Validation, Supervision, Data curation, Conceptualization. **Linqin Peng:** Visualization, Conceptualization. **Haoran Liu:** Visualization, Formal analysis, Conceptualization. **Zhipeng Qu:** Visualization, Formal analysis, Data curation, Conceptualization. **Han Ouyang:** Writing – review & editing, Visualization, Validation, Supervision, Resources, Project administration, Funding acquisition, Conceptualization. **Xu Wu:** Visualization, Software, Data curation, Conceptualization.

Declaration of Competing Interest

The authors declare that they have no known competing financial interests or personal relationships that could have appeared to influence the work reported in this paper.

Appendix A. Supporting information

Supplementary data associated with this article can be found in the online version at doi:10.1016/j.nanoen.2026.111701.

Data availability

Data will be made available on request.

References

[1] H. Singh, H. Kaur, K. Singh, C.K. Sen, Cutaneous manifestations of COVID-19: a systematic review, Adv. Wound Care (N. Rochelle) 10 (2021) 51–80, https://doi.org/10.1089/wound.2020.1309.
[2] R.Z. Luo, Y.J. Fan, Y.L. Qi, Y. Bai, M. Xiao, Y.J. Lv, J.R. Liang, M.C. Tang, J. P. Zhang, Z. Li, D. Luo, Self-manipulating sodium ion gradient-based endogenic electrical stimulation dressing for wound repair, Adv. Mater. 37 (2025) 2419149, https://doi.org/10.1002/adma.202419149.
[3] Y.H. Jiang, Y.J. Zhou, Y. Tian, N. Nabavi, M. Ashrafizadeh, J. Conde, Z. Li, L. Guo, Conductive polymers in smart wound healing: from bioelectric stimulation to regenerative therapies, Mater. Today Bio 34 (2025) 102114, https://doi.org/10.1016/j.mtbio.2025.102114.
[4] Y.Z. Shan, L.L. Xu, X. Cui, J.X. Zhang, H. Ouyang, X.X. Wang, J. Huang, J.T. Xue, K. F. Wang, D.C. Wang, E.G. Wang, K.L. Ren, D. Luo, Z. Li, A neurodevelopment-inspired self-evolving scaffold for nerve regeneration, Cell Biomater. 1 (2025) 100006, https://doi.org/10.1016/j.celbio.2024.100006.
[5] S.R. Barman, S.W. Chan, F.C. Kao, H.Y. Ho, I. Khan, A. Pal, C.C. Huang, Z.H. Lin, A self-powered multifunctional dressing for active infection prevention and accelerated wound healing, Sci. Adv. 9 (2023) eadc8758, https://doi.org/10.1126/sciadv.adc8758.
[6] T.L. Wang, H. Ouyang, Y.P. Luo, J.T. Xue, E.G. Wang, L. Zhang, Z.F. Zhou, Z.Q. Liu, X.F. Li, S. Tan, Y.X. Chen, L.P. Nan, W.T. Cao, Z. Li, F. Chen, L.P. Zheng, Rehabilitation exercise–driven symbiotic electrical stimulation system accelerating bone regeneration, Sci. Adv. 10 (2024) eadi6799, https://doi.org/10.1126/sciadv.adi6799.
[7] W. Pi, H.T. Chen, Y.W. Liu, J.B. Xiang, H.L. Zhang, X.L. Yang, M.R. Zhang, J. W. Cao, T. Chang, Y.F. Zheng, S.Y. Liu, H.J. Zhang, Q. Han, K. Liu, X.B. Fu, Y. Shao, X.Y. Sun, Flexible sono-piezo patch for functional sweat gland repair through endogenous microenvironmental remodeling, ACS Nano (2024) 4c03974, https://doi.org/10.1021/acsnano.4c03974.
[8] C.X. Shi, H. Wang, X.J. Wang, K.F. Li, P.B. Liu, L.H. Wang, H. Yu, A safe, stable, simple, serviceable, and self-powered wound dressing with continuous low-voltage direct current electrical stimulation: an efficient approach to accelerate wound healing, Adv. Funct. Mater. 35 (2025) 2422188, https://doi.org/10.1002/adfm.202422188.
[9] R.Z. Luo, J.Y. Dai, J.P. Zhang, Z. Li, Accelerated skin wound healing by electrical stimulation, Adv. Healthc. Mate 10 (2021) 2100557, https://doi.org/10.1002/adhm.202100557.
[10] Y.N. Sun, Y.F. Tang, Y.X. He, L. Chen, C. Wu, B. Zhang, F.X. Yan, K. Zhao, Z.X. Wu, A self-powered wound dressing based on "Lock-ON/OFF" drug release combined electric stimulus therapy for accelerated infected wound healing, Adv. Funct. Mater. 34 (2024) 2315086, https://doi.org/10.1002/adfm.202315086.
[11] H.J. Qiu, W.Z. Song, X.X. Wang, J. Zhang, Z.Y. Fan, M. Yu, S. Ramakrishna, Y. Z. Long, A calibration-free self-powered sensor for vital sign monitoring and finger tap communication based on wearable triboelectric nanogenerator, Nano Energ. 58 (2019) 536–542, https://doi.org/10.1016/j.nanoen.2019.01.069.
[12] L.L. Xu, E.G. Wang, Y. Kang, D.X. Fu, L. Luo, Y.C. Quan, Y. Xi, J. Huang, X. Cui, J. Zeng, D.J. Jiang, B.J. Shi, H.Q. Feng, H. Ouyang, C.Y. Chen, Z. Li, Schottky nanodiodes array enabled triboelectric nanosecond pulse generator for ultralow-cost tumor therapy, Device 3 (2025) 100721, https://doi.org/10.1016/j.device.2025.100721.
[13] E.G. Wang, M.S. Wu, L. Luo, X. Cui, L.L. Xu, R.Z. Luo, Y. Zou, T. Le, Y.Z. Shan, Y. C. Quan, Y. Bai, L. Wu, Y.R. Hu, S.J. Cheng, J.W. Yang, C. Zhu, D.J. Yu, J.Y. Ji, Y. F. Ren, D.J. Jiang, B.J. Shi, H.Q. Feng, W. Hua, Z. Li, H. Ouyang, Symbiotic biodegradable flexible supercapacitor in vivo, Device 3 (2025) 100724, https://doi.org/10.1016/j.device.2025.100724.
[14] H. Ouyang, D.J. Jiang, Y.B. Fan, Z.L. Wang, Z. Li, Self-powered technology for next-generation biosensor, Sci. Bull. 66 (2021) 1709–1712, https://doi.org/10.1016/j.scib.2021.04.035.
[15] D.J. Jiang, B.J. Shi, H. Ouyang, Y.B. Fan, Z.L. Wang, Z. Li, Emerging implantable energy harvesters and self-powered implantable medical electronics, ACS Nano 14 (2020) 6436–6448, https://doi.org/10.1021/acsnano.9b08268.
[16] Y.Z. Zhang, L.L. Xu, Z. Liu, X. Cui, Z. Xiang, J.Y. Bai, D.J. Jiang, J.T. Xue, C. Wang, Y.X. Lin, Z. Li, Y.Z. Shan, Y. Yang, L. Bo, Z. Li, X.Z. Zhou, Self-powered pulsed

direct current stimulation system for enhancing osteogenesis in MC3T3-E1, Nano Energ. 85 (2021) 106009, https://doi.org/10.1016/j.nanoen.2021.106009.
[17] X.X. Wang, W.Z. Song, M.H. You, J. Zhang, M. Yu, Z.Y. Fan, R. Seeram, Y.Z. Long, Bionic single-electrode electronic skin unit based on piezoelectric nanogenerator, ACS Nano 12 (2018) 8588–8596, https://doi.org/10.1021/acsnano.8b04244.
[18] T.W. Sun, M. Venkatesan, Y.C. Hsu, J. Chandrasekar, W.C. Chen, J.S. Bénas, C. J. Cho, J.H. Lin, F.C. Liang, A.Y. Rwei, C.C. Kuo, MXene-reinforced water insensitive self-healing piezoelectric nanogenerator for ambient and aquatic mechano-pressure sensing, Nano Energ. 133 (2025) 110416, https://doi.org/10.1016/j.nanoen.2024.110416.
[19] M. Venkatesan, J. Chandrasekar, F.C. Liang, W.C. Lin, W.C. Chen, C.J. Cho, Y. T. Chen, W.Y. Lee, C.C. Su, Y. Zhou, Y.C. Lai, C.C. Kuo, Surface-enhanced fully nanofiber-based self-cleanable ultraviolet resistive triboelectric energy harvester for wearable smart garments, Nano Energ. 113 (2023) 108556, https://doi.org/10.1016/j.nanoen.2023.108556.
[20] S.Q. Wang, W.S. Tong, M.T. Tang, Y. Chen, L.P. Lin, J.L. Zhuang, Q. An, J.T. Li, A wireless intelligent patch made of an HAP/PLA@PVDF–HFP fiber film for in situ wound management, Nano Energ. 141 (2025) 111069, https://doi.org/10.1016/j.nanoen.2025.111069.
[21] S.Y. Wang, Z.G. Liu, C. Chen, S.B. Zhang, R.J. Hu, Y.Q. Cao, J. Xu, J.M. Chen, L. W. Yu, Flexible amorphous silicon radial junction patches promote skin regeneration by offering wireless photoelectric neuromodulation, ACS Nano 19 (2025) 18996–19008, https://doi.org/10.1021/acsnano.4c16337.
[22] B.Y. Zhao, J.W. Sun, Y.Z. Xu, J. Li, K.X. Xie, C.C. Zhou, B. Su, L.L. Chen, Programmed temporal modulation by using a magnetoelectric wound dressing for ultra-fast early-stage wound healing, Biomaterials 325 (2026) 123569, https://doi.org/10.1016/j.biomaterials.2025.123569.
[23] J.W. Xin, L.H. Gao, W.J. Zhang, X.Y. Song, Y.M. Yang, W.R. Li, X.H. Zhou, H. Z. Zhang, Z. Wang, Z.X. Wang, B. He, Y.T. Liu, T.Z. Zhou, T. Xiong, S. Wang, S. X. Yuan, W.L. Li, S.C.J. Loo, L. Wang, L. Wei, A thermogalvanic cell dressing for smart wound monitoring and accelerated healing, Nat. Biomed. Eng. (2025), https://doi.org/10.1038/s41551-025-01440-6.
[24] Z. Wang, Q.H. Hu, S.C. Yao, S.B. Wang, X. Liu, C.P. Zhang, Z.L. Wang, L.L. Li, Flexible triboelectric nanogenerator patch for accelerated wound healing through the synergy of electrostimulation and photothermal effect, Small 21 (2025) 2409756, https://doi.org/10.1002/smll.202409756.
[25] J.R. Guo, Y.H. Wei, Z.Z. Guo, T.T. Wang, Y. Ma, H.Y. Li, X. Qin, Y.N. Liu, Z. Wen, P. Miao, Triboelectro-responsive DNA hydrogels for accelerated healing of bacterium-infected diabetic wounds, Nano Energ. 142 (2025) 111217, https://doi.org/10.1016/j.nanoen.2025.111217.
[26] M. Venkatesan, J. Chandrasekar, Y.C. Hsu, T.W. Sun, P.Y. Li, X.T. King, M. A. Chung, R.J. Chung, W.Y. Lee, Y. Zhou, J.H. Lin, C.C. Kuo, Rationally improved surface charge density of triboelectric nanogenerator with TiO2-MXene/polystyrene nanofiber charge trapping layer for biomechanical sensing and wound healing application, Adv. Sci. 11 (2024) 2404019, https://doi.org/10.1002/advs.202404019.
[27] J.L. Li, Z.Y. Che, X. Wan, F. Manshaii, J. Xu, J. Chen, Biomaterials and bioelectronics for self-powered neurostimulation, Biomaterials 304 (2024) 122421, https://doi.org/10.1016/j.biomaterials.2023.122421.
[28] T.H. Cheng, J.J. Shao, Z.L. Wang, Triboelectric nanogenerators, Nat. Rev. Methods Prim. 3 (2023) 39, https://doi.org/10.1038/s43586-023-00220-3.
[29] X. Pu, C. Zhang, Z.L. Wang, Triboelectric nanogenerators as wearable power sources and self-powered sensors, Natl. Sci. Rev. 10 (2023) nwac170, https://doi.org/10.1093/nsr/nwac170.
[30] J.H. Park, C.X. Wu, S. Sung, T.W. Kim, Ingenious use of natural on the human body for versatile applications in walking energy harvesting and body action monitoring, Nano Energ. 57 (2019) 872–878, https://doi.org/10.1016/j.nanoen.2019.01.001.
[31] B.J. Shi, Z. Liu, Q. Zheng, J.P. Meng, H. Ouyang, Y. Zou, D.J. Jiang, X.C. Qu, M. Yu, L.M. Zhao, Y.B. Fan, Z.L. Wang, Z. Li, Body-integrated self-powered system for wearable and implantable applications, ACS Nano 13 (2019) 6017–6024, https://doi.org/10.1021/acsnano.9b02233.
[32] M. Kang, N.Y. Jang, Y.J. Kim, H.J. Ro, D. Kim, Y. Kim, H.T. Kim, H.M. Kwon, J. H. Ahn, B.O. Choi, N.H. Cho, S.W. Kim, Virus blocking textile for SARS-CoV-2 using human body triboelectric energy harvesting, Cell Rep. Phys. Sci. 3 (2022) 100813, https://doi.org/10.1016/j.xcrp.2022.100813.
[33] Y.J. Kim, Z.Y. Huo, X.X. Wang, H.J. Dai, D.M. Lee, I.Y. Suh, J.H. Hwang, Y. W. Chung, H.Y. Lee, Y. Du, W. Ding, S.W. Kim, Walking-induced electrostatic charges enable in situ electroporated disinfection in portable water bottles, Nat. Water 2 (2024) 360–369, https://doi.org/10.1038/s44221-024-00226-5.
[34] L. Yin, K.N. Kim, J. Lv, F. Tehrani, M.Y. Lin, Z.Z. Lin, J.M. Moon, J. Ma, J.L. Yu, S. Xu, J. Wang, A self-sustainable wearable multi-modular E-textile bioenergy microgrid system, Nat. Commun. 12 (2021) 1542, https://doi.org/10.1038/s41467-021-21701-7.
[35] L.B. Xia, H. Zhou, J.K. Chen, F.H. Liu, S.Y. Chang, Y.H. Huang, J.Y. Jiang, K. Dong, Y. Wu, C.H. Zhang, W.P. Xuan, S.R. Dong, J.K. Luo, Human body electrode enabled direct current triboelectric nanogenerator for self-powered wireless human motion and environment monitoring, Adv. Electron Mater. 10 (2024) 2300713, https://doi.org/10.1002/aelm.202300713.
[36] Z.Y. Huo, Y.J. Kim, S.W. Kim, Contact electrification-induced personal sanitation, Nat. Rev. Clean. Technol. (2025), https://doi.org/10.1038/s44359-025-00100-x.
[37] Y. Bai, H.Y. Meng, Z. Li, Z.L. Wang, Degradable piezoelectric biomaterials for medical applications, MedMat 1 (2024) 40–49, https://doi.org/10.1097/mm9.0000000000000000002.
[38] R. Shakibi, F. Yazdipour, N. Imandoost, T. Bajooli, A.A.M. Movahhedi, M. A. Khayamian, Aesthetic, wire-free and bioresorbable dermal tattoo TENG system for self-powered on-the-go biomedical applications, npj Flex. Electron 9 (2025), https://doi.org/10.1038/s41528-025-00473-w.
[39] M. Zhou, M.S.H. Al-Furjan, J. Zou, W.T. Liu, A review on heat and mechanical energy harvesting from human-Principles, prototypes and perspectives, Renew. Sust. Energ. Rev. 82 (2018) 3582–3609, https://doi.org/10.1016/j.rser.2017.10.102.
[40] S.H. Wang, L. Lin, Z.L. Wang, Nanoscale triboelectric-effect-enabled energy conversion for sustainably powering portable electronics, Nano Lett. 12 (2012) 6339–6346, https://doi.org/10.1021/nl303573d.
[41] W.Z. Song, X.X. Wang, H.J. Qiu, Q. Liu, J. Zhang, Z.Y. Fan, M. Yu, S. Ramakrishna, H. Hu, Y.Z. Long, Sliding non-contact inductive nanogenerator, Nano Energ. 63 (2019) 103878, https://doi.org/10.1016/j.nanoen.2019.103878.
[42] X.W. Xiang, H.T. Liu, W. Liu, Z.Y. Yan, Y.L. Zeng, Y.J. Wang, J. Liu, Y.C. Chen, S. X. Yu, C.H. Zhu, X.N. Tao, C. Wang, J.T. Wu, Y. Du, X.X. Xu, H. Gao, Y.M. Jiu, J. Ma, J. Qiu, L.Q. Chang, G.Y. Jing, K.F. Liu, Y.J. Liu, Revolutionizing wound healing: ultrashort pulse electric fields in seconds for highly aligned extracellular matrix and efficient cell migration, Chem. Eng. J. 471 (2023) 144267, https://doi.org/10.1016/j.cej.2023.144267.
[43] X.C. Huang, Q. Zhang, Y.W. Yang, L. Chow, J. Ma, G.Q. Xu, F. Guo, X.X. He, Z.Y. Li, G.Y. Zhao, J.Y. Su, G.H. Guo, J.C. Wang, Y.L. Jiao, Z. Gao, J.Y. Li, J.K. Zhou, C. K. Yiu, J. Li, Y. Chen, P.C. Wu, K.M. Yao, Y.M. Liu, D.F. Li, B.B. Zhang, H.W. Chu, Y. Hu, Y. Huang, Z.L. Chen, K.N. Ren, B. Fang, R.G. Yang, H. Li, X.M. Tao, X.H. Ma, X.G. Yu, A skin-interfaced three-dimensional closed-loop sensing and therapeutic electronic wound bandage, Nat. Commun. 16 (2025) 5782, https://doi.org/10.1038/s41467-025-61261-8.
[44] X. Cui, L.L. Xu, Y.Z. Shan, J.X. Li, J.Y. Ji, E.G. Wang, B.K. Zhang, X.Z. Wen, Y. Bai, D. Luo, C.Y. Chen, Z. Li, Piezocatalytically-induced controllable mineralization scaffold with bone-like microenvironment to achieve endogenous bone regeneration, Sci. Bull. 69 (2024) 1895–1908, https://doi.org/10.1016/j.scib.2024.04.002.
[45] R. Koivuniemi, Q. Xu, J. Snirvi, I. Lara-Sáez, A. Merivaara, K. Luukko, M. Nuopponen, W.X. Wang, M. Yliperttula, Comparison of the therapeutic effects of native and anionic nanofibrillar cellulose hydrogels for full-thickness skin wound healing, Micro 1 (2021) 194–214, https://doi.org/10.3390/micro1020015.
[46] R. Ramakrishnan, D. Chouhan, H.V. Sreelatha, S. Arumugam, B.B. Mandal, L. K. Krishnan, Silk fibroin-based bioengineered scaffold for enabling hemostasis and skin regeneration of critical-size full-thickness heat-induced burn wounds, ACS Biomater. Sci. Eng. 8 (2022) 3856–3870, https://doi.org/10.1021/acsbiomaterials.2c00328.
[47] S. Roy, Z.J. Fan, Z. Ullah, M. Madni, S. Shyamal, J. Roy, N. Bag, L.H. Sun, X. T. Qian, Y.H. Zhang, W. Wang, B. Guo, Ultrasound-powered piezoelectric hydrogel enables dual piezodynamic-chemodynamic therapy and immunomodulation against bacteria-infected burn wounds, Nano Energ. 146 (2025) 111535, https://doi.org/10.1016/j.nanoen.2025.111535.
[48] D. Wu, R.C. Liu, X.T. Cen, W.W. Dong, Q. Chen, J.L. Lin, X. Wang, Y.X. Ling, R. Mao, H.T. Sun, R. Huang, H.X. Su, H.J. Xu, D.J. Qin, Preclinical study of engineering MSCs promoting diabetic wound healing and other inflammatory diseases through M2 polarization, Stem Cell Res. Ther. 16 (2025) 113, https://doi.org/10.1186/s13287-025-04248-y.
[49] X.X. Shi, B.Y. Peng, X. Cai, S.D. Zhang, Y.X. Chen, Ultrasound-enhanced piezoelectric nanogenerators for wireless electrostimulation therapy in the wound healing, Nano Energ. 139 (2025) 110940, https://doi.org/10.1016/j.nanoen.2025.110940.
[50] S.X. Xu, H.W. Shao, Z.Y. Jin, J.K. Xu, F.Y. Deng, Y.T. Zhang, L.B. Zhou, S.K. Ling, C. Q. Ning, W.X. Tong, L. Qin, Magnesium silicate composite patch with neurovascular regenerative properties promotes diabetic wound healing in mice, Inter. Mater. 4 (2025), https://doi.org/10.1002/idm2.70003.